

**AIRSHIP**

Funded by the European Union's  
Horizon Europe programme under  
the grant agreement No 101096487



# **D4.1 Full set of electrical specifications for the propulsion DC Microgrid**

## **WP4 Power Plant and Power Management**

## Disclaimer

The content of this deliverable reflects only the author's view. The European Commission is not responsible for any use that may be made of the information it contains.

## Document Information

Grant Agreement / Proposal ID	101096487
Project Title	AUTONOMOUS FLYING SHIPS FOR INTER-ISLAND AND INLAND WATERS TRANSPORT
Project Acronym	AIRSHIP
Project Coordinator	Universidad Politécnica de Madrid
Project starting date (duration)	1st January 2023 (48 months)
Related Work Package	WP4
Related Task(s)	T4.1
Lead Organisation	UPM
Contributing Partner(s)	TAU
Due Date	31.12.2023
Submission Date	31.12.2023
Dissemination level	Public

## Revision History

Revision	Revision Date	Name	Position
1	December 20 <sup>th</sup> , 2023	Pedro Alou	Researcher
2	December 30 <sup>th</sup> , 2023	Jussi Aaltonen	Researcher



## TABLE OF CONTENTS

1	Introduction .....	6
2	Review of Technologies applicable to the propulsion DC Microgrid .....	6
2.1	Propeller technologies for WIG crafts .....	6
2.2	DC Microgrid Architecture .....	7
2.2.1	Ring Configuration .....	8
2.2.2	Radial Configuration .....	9
2.2.3	Protection under faults and disturbances.....	10
2.3	Energy generation and storage technologies.....	11
2.4	Electric propulsion technologies .....	15
3	Definition of different usage scenarios .....	16
4	Airship-1 scenario .....	17
4.1	Mechanical requirements.....	17
4.2	Electric motor requirements.....	19
4.3	DC Microgrid Architecture .....	21
4.4	DC Microgrid dynamic requirements.....	21
4.4.1	Current control.....	22
4.4.2	Voltage control .....	25
4.5	Energy generation and storage requirements .....	29
	Different technologies and configurations have been studied as show below.....	29
4.6	DC protections .....	30
4.6.1	Fault detection .....	31
4.6.2	System response.....	31
5	Full DC Microgrid Architecture for AIRSHIP A-1: Lab demonstrator .....	32
5.1	DC Microgrid Architecture .....	32
5.2	Energy generation and storage requirements .....	33
5.3	Full DC Microgrid: Dynamic requirements and grid stability.....	35
5.3.1	Taking off.....	36
5.3.2	Cruise.....	37
5.3.3	Landing.....	38
5.4	DC protections and redundancy .....	38
6	Conclusions .....	39



## List of Tables

Table 1. Abbreviation and Acronyms .....	4
Table 2. Lithium based battery technologies. ....	14
Table 3 Usage scenarios considered in AIRSHIP project.....	17
Table 4 Motor specifications .....	20
Table 5 Controller specifications .....	20
Table 6 DAB converter specifications for A1.....	23
Table 7 Power consumption.....	29
Table 8 Analysed commercial batteries for the Navigation and control system .....	29
Table 9 Analysed commercial batteries for the Propulsion of AIRSHIP-1 demonstrator.....	30
Table 10 Power consumption in A-1 .....	33
Table 11 Analysed commercial Batteries for the Lab Demonstrator .....	34
Table 12 Fuel Cell specifications for the Lab Demonstrator.....	34
Table 13 Supercapacitors specifications for the Lab Demonstrator .....	35
Table 14 PV panel design.....	35

## List of Figures

Figure 1 Total drag curve of A-1 at different stages of flight. [Deliverable D3.1] .....	7
Figure 2. Option A1: single battery and fuel cell configuration.....	8
Figure 3. Option A2: double battery and fuel cell configuration.....	8
Figure 4. Option B1: Independent 28V buses with single propulsion battery and fuel cell. ....	9
Figure 5. Option B2: Independent 28V buses with double propulsion batteries and fuel cells. ....	9
Figure 6. 28V bus alternative configuration to increase redundancy in the system. ....	9
Figure 7. Option C1: single battery and fuel cell configuration.....	10
Figure 8. Option C2: double battery and fuel cell configuration.....	10
Figure 9. Option D1: single battery and fuel cell configuration.....	10
Figure 10. Option D2: double battery and fuel cell configuration.....	10
Figure 11. Generation and storage technologies.....	11
Figure 12 Comparison of the control of BLDC and PMSM motors.....	16
Figure 13 APC 25x12.5E thrust at 6000 r/min as a function of relative air velocity [APC propellers].....	18
Figure 14 RPM and thrust required of A-1 at different stages of flight. [APC propellers, Deliverable D3.1] .....	18
Figure 15 Candidate BLDC motor for AIRSHIP-1 prototype .....	19
Figure 16 Block diagram: Motor and its controller .....	20
Figure 17 AIRSHIP –1: Proposed DC Microgrid Architecture .....	21
Figure 18 Dual active bridge (DAB) DC/DC bidirectional converter .....	22
Figure 19 Average circuit of Dual active bridge (DAB) DC/DC bidirectional converter.....	22
Figure 20 Bode analysis for the current PI controller .....	23
Figure 21 DAB input current simulation with PI controller .....	24
Figure 22 DAB input current simulation with nonlinear controller.....	25
Figure 23 Bode diagram for voltage controller.....	26
Figure 24 Voltage of DC grid in voltage control mode.....	26



Figure 25 Input current ( $i_1$ ) of DAB in voltage control mode .....	27
Figure 26 Four nodes DC grid .....	27
Figure 27 a) Input current of DAB 1 b) Input current of DAB 3 .....	28
Figure 28 Voltage of the DC grid in the four nodes grid simulation .....	28
Figure 29 Solid State DC Circuit Breaker .....	31
Figure 30 Full DC Microgrid Architecture for AIRSHIP-1: Lab demonstrator .....	33
Figure 31 DC Microgrid architecture modelled to analyse dynamic requirements .....	36
Figure 32 Input current of the DAB converter within the Full DC Microgrid simulation during the take off.....	36
Figure 33 Voltage of the DC Bus within the Full DC Microgrid simulation during the take off. ....	37
Figure 34 Input current of the DAB within the Full DC Microgrid simulation during the cruise. ....	37
Figure 35 Voltage of the DC grid within the Full DC Microgrid simulation during the cruise.....	38
Figure 36 Input current of the DAB within the Full DC Microgrid simulation during the landing. ....	38
Figure 37 AIRSHIP –1: Proposed DC Microgrid Architecture .....	39
Figure 38 Full DC Microgrid Architecture for AIRSHIP-1: Lab demonstrator .....	39
Figure 39. EU Flag. ....	43

## Abbreviations and Acronyms

Acronym	Description
DAB	Dual Active Bridge converter
WIG	Wing in Ground effect

Table 1. Abbreviation and Acronyms



## EXECUTIVE SUMMARY

This deliverable corresponds to WP4 and presents the electrical specifications for the propulsion DC Microgrid. First, a review of the DC Microgrid technologies like DC architectures, batteries, fuel cells, supercapacitors, electrical motors and Circuit Breakers is presented. Then, electrical specifications for the AIRSHIP scenarios are presented. Based on this scenarios, two demonstrators are identified: AIRSHIP-1 and Full DC Microgrid AIRSHIP-1 Lab demonstrator. A DC Microgrid architecture is proposed for each demonstrator, providing a preliminary design for the main parts of the DC Microgrid. Based on this preliminary design for the DC Microgrid of each demonstrator, the dynamic requirements and the stability of the DC Microgrid is analysed by developing the required dynamic models and running the corresponding simulations to verify the properly behaviour and stability of the DC Microgrid during the take-off, cruise and landing. Once the rest of WPs of the project provide a more detailed models of the AIRSHIP-1 prototype, the final dynamic requirements will be defined with high accuracy; regardless the final dynamic requirements are very demanding or not, two control techniques based on Linear control and Non-linear control, have been analysed and presented. The Linear Control shows appropriate behaviour if the dynamic requirements are low; in the case of demanding dynamic requirements, Non Linear control has shown appropriate behaviour and would be the selected one.



# 1 Introduction

This deliverable is focused on the Power Plant of the Wing-in-Ground effect craft, being the main purpose to define and specify the architecture and required technologies of the propulsion DC Microgrid. Firstly, the technologies needed to develop the propulsion DC Microgrid are reviewed.

The AIRSHIP usage scenarios are defined and initial electrical specifications for taking-off, cruise and landing are provided for the different scenarios based on preliminary simulations and models.

Based on these preliminary specifications, the Power Plant demonstrators to be developed within AIRSHIP project are identified.

A preliminary design is proposed covering: mechanical requirements (thrust and propeller rotational speed), electrical motor (power specs), on-board energy storage elements (batteries, fuel cells and supercapacitors), off board energy and hydrogen generation (PV panels and electrolyzer), DC microgrid architecture accounting for reliability (redundancy, failure detection and isolation).

## 2 Review of Technologies applicable to the propulsion DC Microgrid

### 2.1 Propeller technologies for WIG crafts

Propeller requirements of the wing-in-ground effect (WIG) craft differ significantly from the conventional aircraft. This is because of the difference in total resistance during the take-off. In conventional aircraft the total resistance consists of the aerodynamic resistance and the rolling resistance. In the WIG components of the total resistance are aerodynamic and hydrodynamic resistance. The hydrodynamic resistance is higher than the rolling resistance would be and it also has higher velocity dependence. Because of this WIG crafts (and seaplanes in general) require propellers which have capability to produce high thrust in low relative air speed region.

A flight operation has following distinct stages: displacement mode, hydroplaning mode, take-off, cruise flight and landing. Power required changes greatly depending on the stage of the operation. At displacement mode the WIG craft moves in water supported by buoyancy of the floatwing. At this state the craft operates like conventional displacement hull boat and its hydrodynamic resistance is high. When the craft's velocity increases happen transition to the hydroplaning mode. At this mode only trailing edge of the wing root section is in contact with water and majority of the craft's weight is supported by hydrodynamic lift. In hydroplaning mode, the total resistance is greatly reduced from the displacement mode. When the velocity increases greater proportion of the crafts weight becomes supported by the aerodynamic lift, until take-off speed is reached, and the craft begins to fly. When airborne, craft accelerates to cruise speed which is the most economical flight speed.

When total drag  $D_{tot}$  is known at each stage of operation, power required  $P$  can be calculated using the equation:

$$P = \frac{vD_{tot}}{\mu_{prop}} \quad (1)$$



Where  $v$  is the speed variable through the stages and  $\mu_{prop}$  is propeller efficiency. Drag generated and power by A-1 craft at different speeds is estimated in Figure 1. Note that hydroplaning begins at around speed of 7m/s and takeoff at about 19m/s.

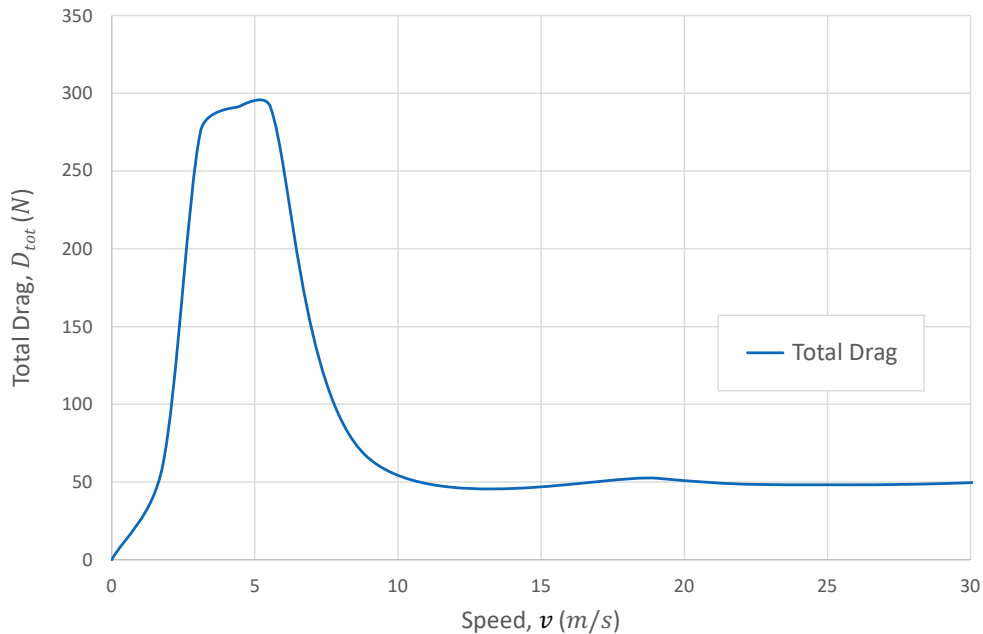


Figure 1 Total drag curve of A-1 at different stages of flight. [Deliverable D3.1]

Figure 1 shows that the required minimum thrust needs to be approximately 300N for the speed range of approximately 3–6 m/s. To achieve sufficient acceleration, thrust needs to be somewhat higher than that.

## 2.2 DC Microgrid Architecture

In recent years, DC microgrids have emerged as alternative to classical AC distribution networks. In a similar way, the solutions for aircraft electrical grids are also moving from AC grids to DC grids due to some strategic considerations (Dragicevic, 2018):

- **DC micro grids presents better efficiency and easy integration with renewable sources:** such as solar panels due to their inherent compatibility with DC. This allows for more efficient power conversion and usage.
- **Simplified power electronics:** as it reduces the need for complex and heavy AC/DC conversions and minimizes the number of power electronics elements. This not only enhances overall efficiency but also contributes to a lighter and more compact design. This also reduces transmission losses.
- **Enhanced control and stability:** providing precise control over voltage levels and facilitating energy management.
- **Safety and redundancy:** DC systems offer easier fault detection and isolation mechanisms. In the event of a fault, the impact can be minimized, contributing to the safety measures required for aviation applications.



DC/DC converters are implemented between the grid elements and adapt the voltages to the desired values. Unidirectional or directional character of each converter is decided based on power economy. The selected bidirectional converter is Dual Active Bridge topology (DAB), since this topology provides, high conversion ratio, high power efficiency and bidirectional flow, for example, between the battery and the grid for battery discharge or charge depending on the power requirements of the grid. DAB is also selected in the motors' node for regenerative braking scenarios.

There are two main options for DC microgrid architecture that align with the prototype requirements, and inside those two configurations, two more options of DC buses distribution:

### 2.2.1 Ring Configuration

Ring configurations consist of a closed-loop topology where each component is adjacent to its counterparts. Power can flow in both directions within the loop allowing bidirectional flow.

In this configuration, nodes are connected through intelligent electronic devices (IDEs). This type will increase the reliability of the system. It allows easy equipment maintenance during fault conditions. And its main advantage is that during fault conditions alternative paths are available for the power flow.

This way, this configuration allows effective fault isolation, if a fault occurs it can be contained within a specific segment preventing it from affecting to the entire structure. However, this interconnected nature can introduce complications in system management and control as well as increased weight implications due to the extra wiring.

For the ring configuration, as well as the radial one, two main options are presented: including avionics and flight control nodes into the microgrid or keeping them separate with auxiliar batteries. Apart from these two options, another two configurations for the main battery and fuel cell arise: having only one of each or duplicating them, keeping the overall power the same and halving the individual power supply. Ahead some of the options are presented:

#### Option A: Ring microgrid with main 400V bus and two integrated 28V buses:

This option incorporates all the microgrid components into a single ring configuration. The avionics and flight control nodes will be connected to the grid with a 400/28V isolated DC/DC converter.

**\*Note:** the electrolyzer is part of the off-board grid and it is only represented in the following architectures that are focused on the on-board power plant.

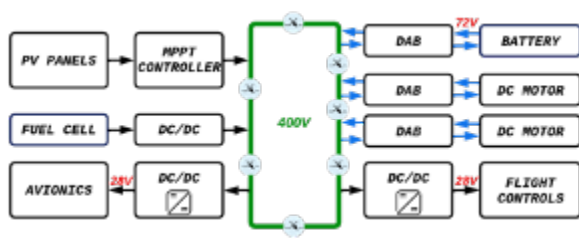


Figure 2. Option A1: single battery and fuel cell configuration.

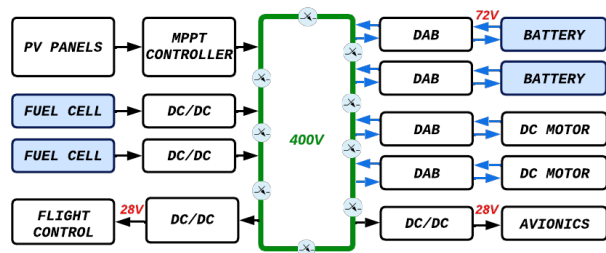


Figure 3. Option A2: double battery and fuel cell configuration.

#### Option B: Ring microgrid with two independent 28V buses:

This option consists of the separation of the auxiliary buses from the main 400V bus. Isolating them from the microgrid and implementing two additional batteries. Separating the buses means reducing the dependency of



the main grid, resulting in better reliability of the system. However, this method means using two additional batteries, which implies a drastic weight increase.

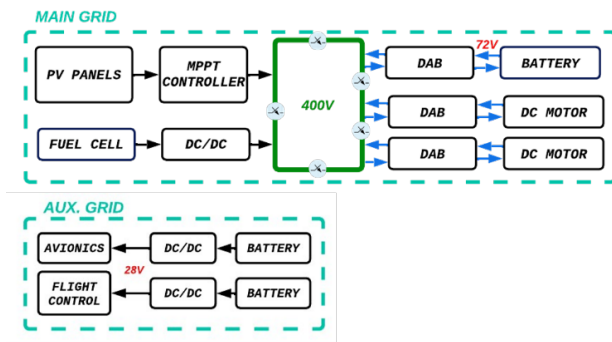


Figure 4. Option B1: Independent 28V buses with single propulsion battery and fuel cell.

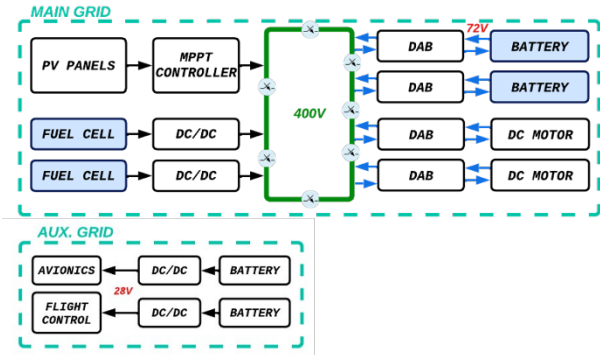


Figure 5. Option B2: Independent 28V buses with double propulsion batteries and fuel cells.

Separating the flight control and avionics supplies from the grid, brings new options and configurations to the table. For example, implementing a more redundant 28V bus like it is shown in the following figure.

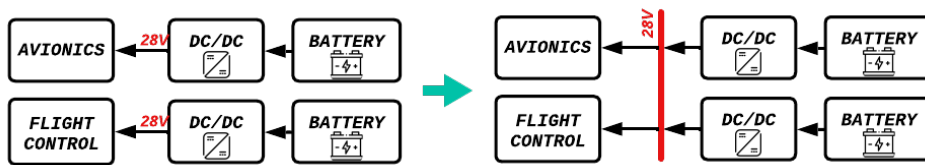


Figure 6. 28V bus alternative configuration to increase redundancy in the system.

## 2.2.2 Radial Configuration

Radial microgrid configurations provide a simpler approach as well as an easier implementation as the principal bus only has one main node. This simplicity does not mean less redundancy, as it depends mainly on the node isolation system. The node isolation can be achieved with two different techniques:

- Using the DC/DC converters as circuit breakers: this technique consists of using the converter's MOSFET transistors as circuit breakers, synchronizing their opening in case of a fault.
- Using independent circuit breakers in series with the converters: this is the safest option as well as the easiest to control.

### Option C: Radial microgrid with 400V main bus and two integrated 28V buses:

This option incorporates all the microgrid components into a radial configuration. The avionics and flight control nodes will be connected to the grid with a 400/28V isolated DC/DC converter.



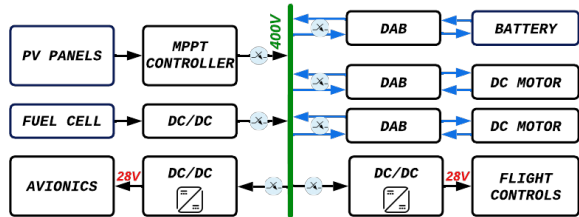


Figure 7. Option C1: single battery and fuel cell configuration.

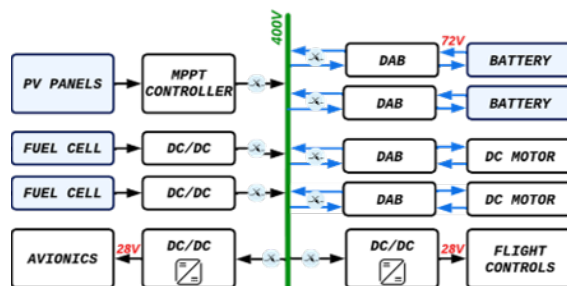


Figure 8. Option C2: double battery and fuel cell configuration.

### Option D: Radial microgrid with 400V main bus and two independent 28V buses:

This option is equivalent to Option B where auxiliary buses are separated from the main 400V bus, being Radial the microgrid configuration. As mentioned above, separating the buses means reducing the dependency of the main grid, resulting in better reliability of the system.

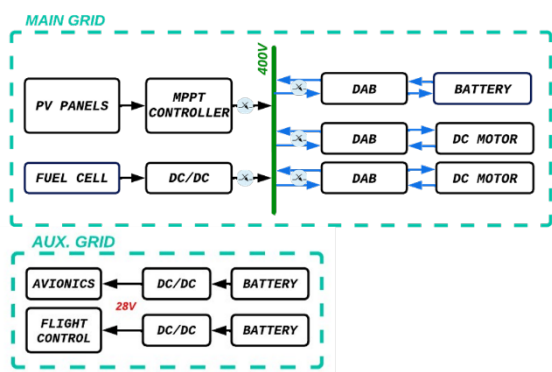


Figure 9. Option D1: single battery and fuel cell configuration.

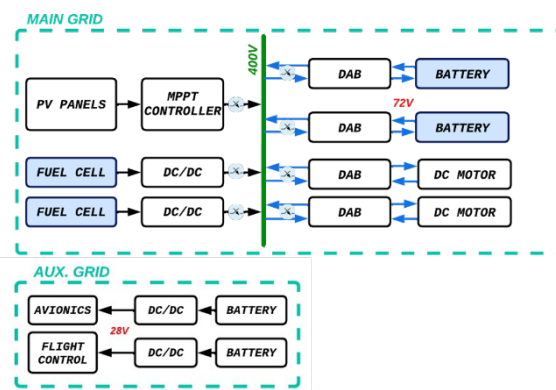


Figure 10. Option D2: double battery and fuel cell configuration.

### 2.2.3 Protection under faults and disturbances

Due to the low inertia and converter behaviour, the microgrid system is potentially very sensitive to disturbances and faults. Another issue with the DC microgrid protection design is the discrimination of faults and other disturbances. To achieve a better performance, the protection schemes should categorize the disturbances (like sudden changes in the source power, load, parametric variations, errors in the voltage and current feedback etc.) and faults as temporary or permanent.

The following DC protection devices are considered:

- Sensors and snubbers: The power converters incorporate MOSFET or IGBT-based devices, which have high switching frequency and high current and voltage withstanding capabilities. By using additional circuits (snubbers), these devices can improve their performance, reducing voltage transients and improving system reliability.
- Protective relays: DC power relays can protect from overvoltage, overcurrent, ground faults, etc. Combined with sensors, if the measured values deviate from a threshold value for a longer time period



than a certain limit, a trip signal will be sent to the contactors to isolate the fault. Digital relays are popular because they can monitor and protect from more than one fault condition. The IEEE standard for AC relays is C37.90-2005-IEEE.

- Circuit Breakers: following IEEE STD C37.14-2015 and LVSD-WG\_C37.16-LVSD standards. The most efficient type is Solid State DC Breakers, thanks to their high switching speed, full controllability and high blocking and carrying capacities.

There is also the need to define a fault classification protocol and emergency state. Determining which faults are considered temporary or permanent and their grade. The emergency protocol will depend on the architecture decision, in the double battery and fuel cell options for example, in case a battery fails, the grid can still be powered with the second one, working with half the power flow and allowing the vehicle to float to port for reparations.

### 2.3 Energy generation and storage technologies

Traditionally microgrids have been powered with carbon-based fuels generation, and therefore the main storage element were tanks. Nowadays, zero CO<sub>2</sub> net emission energy sources are an alternative solution.

It must be noticed that there are two main grids one located on-board and another one off-board used only in the loading and unloading process to refill the H<sub>2</sub> tank and recharge the batteries. In this document only the on-board grid is described in detail while some guidelines are included about the off-board grid.

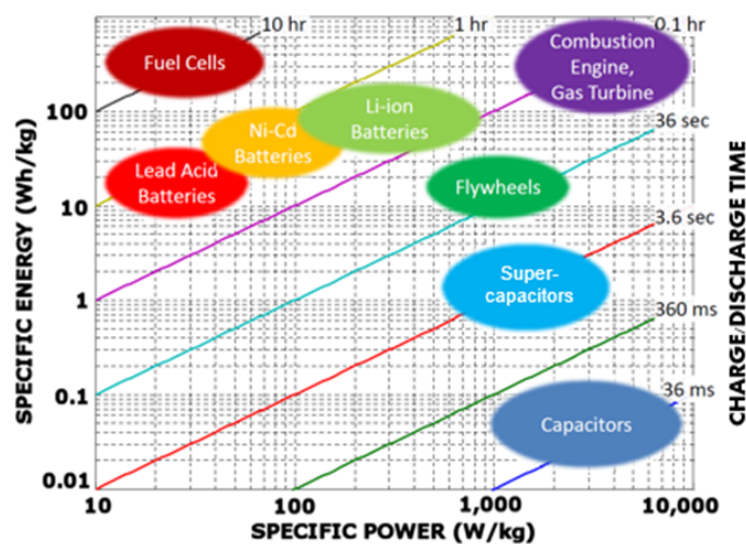


Figure 11. Generation and storage technologies.

There are only two elements that are not present in the on-board grid: the bidirectional inverter to connect the DC grid to the AC power grid, and the electrolyser to generate green H<sub>2</sub>. To scale the elements of the off-board grid, it would be necessary to estimate the number of WIG crafts and its frequency of use, which is out of scope of this project.

For the on-board grid the energy generation is produce by PV panels and a fuel cell, the energy storage is distributed between batteries, supercapacitors and a H<sub>2</sub> tank. The combination of selected technologies as well as percentage of energy/power manage by each technology depends on the power consumption profile, the peak to average power demand and the duration of high power demand operations like take off. In the above figure, a comparison of different topologies taking into account the power density and the energy density is shown.



In case of having an almost constant energy consumption the most suitable technology is fuel cells, therefore during cruising this will be the primary energy source, the extra energy needed during take off will be supplied by batteries. To improve the dynamic of the DC grid, supercapacitor will be included to feed the grid during very small bursts of power.

More details about the different power sources and energy storage elements are discussed below.

### 2.3.1.1 Photovoltaic panels

Solar cells, also called photovoltaic cells, convert sunlight directly into electricity. This phenomenon was first exploited in 1954 by scientists at Bell Laboratories who created a working solar cell made from silicon that generated an electric current when exposed to sunlight.

Solar energy harvesting based on photovoltaic technology provides a power density of around 15mW/cm<sup>2</sup> on bright sunny days. Depending on the technology, the achieved efficiency varies:

- Monocrystalline: This type of cells presents the highest conversion efficiency in the market; it is the more mature technology and has a high reliability. The efficiency is around 15-24%
- Polysilicon: Has considerably lower cost than monocrystalline but presents lower efficiency (14-20.4%)
- Amorphous silicon (a-Si): It is a cheap technology, with very low dark conductivity and a good response to weak light. The main drawback it is its limited efficiency (8-13.2%)
- Cadmium Telluride (CdTe): Theoretically this technology presents a 28% efficiency, high light absorption rate, and stable performance. But nowadays is a costly technology and has toxic materials.
- Copper-indium-gallium-diselenide(CIGS): Its efficiency is up to 20%. It is a low cost technology with a good weak light performance, wide applicability of substrate, adjustable optical bandgap, strong antiradiation ability. However, is made of rare materials and it is difficult to control four elements precisely.

It will be considered the idea of placing the PV over the wing surface, to maximize the irradiance and the used area. Another point that must be taking into account is the weight of the PV panels, in general it is around 11.4 kg/m<sup>2</sup>

### 2.3.1.2 Fuel cells

Fuel cell invention was made in the middle of the 19<sup>th</sup> century by Sir William Grove. A fuel cell uses the chemical energy of hydrogen or other fuels to cleanly and efficiently produce electricity. If hydrogen is the fuel, the only products are electricity, water, and heat.

Fuel cells are classified primarily by the kind of electrolyte they employ. This classification determines the kind of electro-chemical reactions that take place in the cell, the kind of catalysts required, the temperature range in which the cell operates, the fuel required, and other factors.

- Alkaline Fuel Cells: The AFC has the highest efficiency but only works properly with very pure gases. The KOH electrolyte has an advantage over acidic fuel cells. The oxygen reduction kinetics are much faster. The temperature operation range is between 60 °C to 90 °C. Its main drawback is that is not tolerant to CO<sub>2</sub>.
- Proton Exchange Membrane Fuel Cells. PEM fuel cells use a proton-conducting polymer membrane as an electrolyte. They generally operate at 85-105°C. Polymer Electrolyte Membrane (PEMFC) is a specific



type of PEM that present fast start-up and no leakage of electrolyte. However, this technology is not CO tolerant and presents some problems with the water management in membranes.

- Direct Methanol Fuel Cells: DMFC is a type of PEM fuel cell. It operates at temperatures similar to PEMFC although it can also run at slightly higher temperatures. Its main advantage is that methanol is easier to store. But it does not solve the other drawbacks of PEM fuel cells.
- Molten Carbonate Fuel Cells: MCFC as all carbonaceous fuels will produce CO<sub>2</sub> along their oxidation, but it is able to internally reform methane due to the high operating temperatures (600-700 °C). This technology has the advantage of high efficiency, especially combined with gas turbine.
- Solid Oxide Fuel Cells: SOFC technology employs a solid oxide material as electrolyte and is more stable than MCFC: However, it is difficult to find suitable materials which have the necessary thermal and chemical stability properties for operating at high temperatures (800-1000 °C).

For the application under study the most suitable technology is PEM fuel cells, this technology is widely used in vehicles.

### 2.3.1.3 Batteries

A battery is a device composed by one or more electrochemical cells that due to a chemical reaction create an electrons flow. The battery properties depend highly on the battery chemistry type. The invention of the battery as we know was in 1800 by Alessandro Volta. Since then, several types of batteries have been developed and the most used ones are listed below pointing out its main characteristics:

- Lead–Acid (PbA) Battery: This type of batteries presents a low-cost and simple manufacture, a high specific power, capable of high discharge currents and a good performance at wide temperature range but they have a low specific energy, cannot have a fast charging and present limited cycle life.
- Nickel–Cadmium (Ni–Cd) Battery: There are a wide range of sizes and performance options of this type of batteries. It presents an ultra-fast charged capability with little stress and has an economical price. Anyhow, it has a relatively low specific energy and low cell voltage therefore several cell must be stacked to obtain high voltage levels.
- Nickel–Metal Hydride (Ni–MH) Battery: It presents higher capacity and less voltage depressing compared to other rechargeable batteries, but it has limited-service life and limited discharge current in repetitive mode. It also needs for a more complex charge algorithm and presents a high self-discharge.
- Lithium-Ion (Li-Ion) Battery: The main advantages of this technology are that it has the highest energy density and is considered safe. It also presents high load capability, and long cycle and extended shelf-life, as well as simple charge algorithm and reasonably short charge times. But it needs for protection circuit to prevent thermal runaway under abnormal conditions.
- Lithium-polymer (LiPo) Battery: Is a specific type of Li-Ion battery lighter and more flexible than other kinds of Li-Ion batteries. It offers high specific energy, and high capacity and hence can be used to hold



more power. But it supports less recharge life cycles, requires special care during charging, discharging and storage, and the cost is almost double that Li-Ion battery.

- Sodium–Sulfur (Na–S) Battery: It exhibits low losses during charge and discharge and high energy density as well as long cycle life. On the other hand, it has a high operating temperature above 300°C.
- Redox Flow Battery (RFB): this type of batteries has long service life, high safety and has a versatile design, however, presents a low energy density and a high complexity as it composed of pumps, sensors, flow and power management, ...

Taking into account the different technologies presented above, the most suitable for the application of this project is the Lithium-Ion technology or Lithium-polymer technology depending on the life cycle and the payload of the UAV. There are a wide range of Lithium-Ion batteries, the main characteristic of the most used technologies in the industry are summarized in the table below.

Table 2. Lithium based battery technologies.

Lithium-Ion Battery Type	Energy Density (Wh/kg)	Advantages	Disadvantages
Lithium Titanate (LTO)	50-80	Long life, stable	Low energy density, more expensive.
Lithium Cobalt Oxide (LCO)	150-200	High energy density	Volatile and expensive.
Lithium Nickel Manganese Cobalt Oxide (NMC)	150-220	High energy density	Relatively unstable and expensive.
Lithium Iron Phosphate (LFP)	90 -160	Stable, durability and long life cycle	Lower operating voltage than other lithium-ion. Reduced performance at low temperature.

For the application under study the most suitable one is a lithium iron phosphate battery which presents a good compromise between energy density and reliability.

#### 2.3.1.4 Supercapacitors

Supercapacitor is a type of energy storage components, its function lies between the battery and the electrostatic capacitor, and has a great power density, high charging efficiency. Therefore, in industrial production, it can be used for fast energy storage due to its high-power density. Supercapacitors have much higher capacitance values compared to the other capacitor types and are available in values of a tenth of a Farad to several thousand Farads. Individually, they have lower voltage limits than electrolytic capacitors, about 2 V to 4 V.

Comparing batteries and supercapacitors, while batteries can provide ~10x more energy over much longer periods of time than a supercapacitor can (meaning they have a higher specific energy), supercapacitors can deliver energy ~10x quicker than a battery can (meaning they have a higher specific power).



## 2.4 Electric propulsion technologies

There are several technologies when it comes to electric propulsion. In this section, a brief overview of them is done.

The simplest motor technology is the **DC motor**. This type of motor relies on brushes and a commutator for current direction switching and generate power. These motors are simple, therefore, its control methods are not complex. Although cost-effective, they need regular maintenance due to brush wear. DC motors are suitable in applications where cost is a primary consideration, and precise control and performance are not priorities.

**Induction AC motors** utilize electromagnetic induction to create a magnetic field in the rotor. This operational principle requires a rotational speed difference between the stator magnetic field and the rotor. These motors exhibit simplicity and robustness, yet they tend to have lower efficiency compared to other motor types. Additionally, they permit less precise control. Induction AC motors find suitability in applications where cost and simplicity take precedence over efficiency.

**Permanent magnet motors** employ magnets on the rotor to create a magnetic field synchronized with the field generated in the stator. Distinguished by high power density and efficiency, these motors demand minimal maintenance and offer precise controllability, albeit at a higher cost. The two principal subtypes are BLDC (Brushless DC motor) and PMSM (Permanent magnets synchronous motor), differing primarily in winding distribution and control methods. The BLDC subtype is characterized by simplicity, while the PMSM subtype offers better performance but has a more complex control, as illustrated in the accompanying figure.

- **Brushless DC motors:** their control electronics are designed to execute trapezoidal commutation, a requirement imposed by the trapezoidal back electromotive force generated in the stator winding due to its specific winding pattern. This trapezoidal configuration introduces torque ripple during each commutation, consequently diminishing the overall torque output. Moreover, these motors are known for generating acoustic and electric noise.
- **Permanent magnets synchronous motors:** Sinusoidal commutation is utilized in Permanent Magnet Synchronous Motors (PMSM) because of the inherent sinusoidal back EMF in these motors. The basic principle of sinusoidal commutation involves providing sinusoidal currents that adapt to the rotor's position, with a 120-degree phase shift between them. Achieved through a Field-Oriented Control Algorithm, this approach optimizes torque production by adjusting the sinusoidal current according to the rotor's position.

The following figure shows the different control waveforms required for BLDC and PMSM motors that are most appropriate for the scenarios considered in this project.



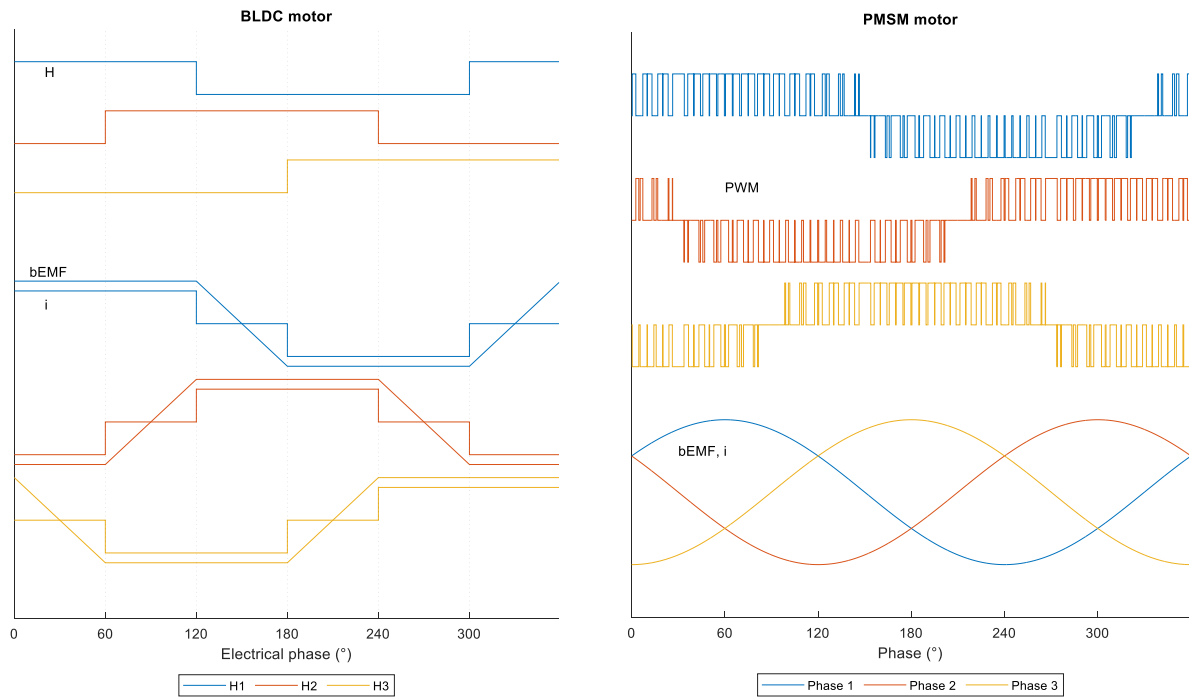


Figure 12 Comparison of the control of BLDC and PMSM motors

Another important consideration for the choice of motors in these types of applications is the ability of the motor to regulate its rotation speed in a simple way. It is also important to note that the motor propeller can be, in general, with variable or fixed pitch, which will affect the lift of the airplane and consequently the control of the rotation speed of the motor. For simplicity, for the A-1, a constant pitch propeller will be implemented, which means that the lift will depend almost exclusively on the rotation speed of the motor.

### 3 Definition of different usage scenarios

The following table shows the three scenarios considered within AIRSHIP project. A0-S is a first basic prototype to be developed in the project that will allow to do preliminary tests of the implemented technologies as well as obtain measurements and data to improve the accuracy of the models. From the point of view of the power plant, it will be very useful to verify energy and power demanded by the aircraft during the take-off in comparison with the energy and power needed during the cruise.

AIRSHIP-1 (A-1) is the small-scale prototype to be developed along this project to validate most of the technologies needed in the Air Ship. This scale is higher than the A0-S and is high enough to do a representative validation of the required technologies.

Finally, the Commercial Concept (CC) gives the specifications of a considered business case at real scale.

In the following sections, it is presented, from the Power Plant perspective, the specifications for the demonstrators that must be designed, built and tested to validate the technologies to be developed as well as the main challenges.



Table 3 Usage scenarios considered in AIRSHIP project

Parameter	Symbol	CC	A-1	A0-S
Linear scale factor	–	1,0	0,2	0,1
Wing span	$b$	25,0 m	5,0 m	2,5 m
MTOW	$m_t$	12 000 – 16 000 kg	100 – 120 kg	10 – 14 kg
Cruise speed	$v_c$	210 – 234 km/h	97 – 108 km/h	38 – 47 km/h
Cruise total motor power	$P_c$	350 – 800 kW	1,5 – 3,5 kW	–
Take-off speed	$v_{to}$	120 – 140 km/h	65 – 72 km/h	–
Take-off total motor power	$P_{to}$	550 – 1000 kW	2,7 – 4,5 kW	–
Range	$d_r$	1000 km	–	–
Cargo space length	$l_{cs}$	7,93 – 10,0 m	–	–
Cargo space width	$w_{cs}$	2,22 m	–	–
Cargo space height	$h_{cs}$	1,88 m	–	–
Payload	$m_{pl}$	4 000 – 7 000 kg	20 kg	–
Lift-to-drag ratio	$L/D$	18,5	–	–
Take off time	$t_{to}$	30 s	20 s	–
Cruising time	$t_{cr}$	1 – 2 hours	10 min	–
Landing time	$t_{ln}$	30 s	20 s	–

## 4 Airship-1 scenario

The main aim of AIRSHIP-1 prototype is to test and validate mechanical and flight aspects, navigation and autonomous control of the WIG craft. Therefore, the main goal of the Airship-1 DC Microgrid is simplicity and robustness to make sure that the needed energy and power is available and properly delivered during the different operation modes and flight tests. In the following sections, the specifications for the different parts of the DC Microgrid are presented having robustness and simplicity as the main drivers and being weight another key parameter to be regarded.

### 4.1 Mechanical requirements

The most essential requirement for propellers of AIRSHIP A-1 prototype is ensuring the take-off capability of the craft. The hydrodynamic drag is the largest component of the total drag for take-off speed range and the propeller thrust capability needs to have enough reserve to provide necessary acceleration to achieve adequate take-off time and take-off distance.

Figure 1 in the Chapter 2.1 shows the thrust requirement for the propellers. Considering a propeller rotational speed of 6000 r/min a suitable propeller, which could fulfil the thrust requirement is for example APC Propellers 25x12.5E. It is a 2-bladed glass fibre composite propeller with a diameter of 0,635m. Figure 13 shows the thrust of the mentioned propeller at 6000 r/min as a function of relative air velocity.



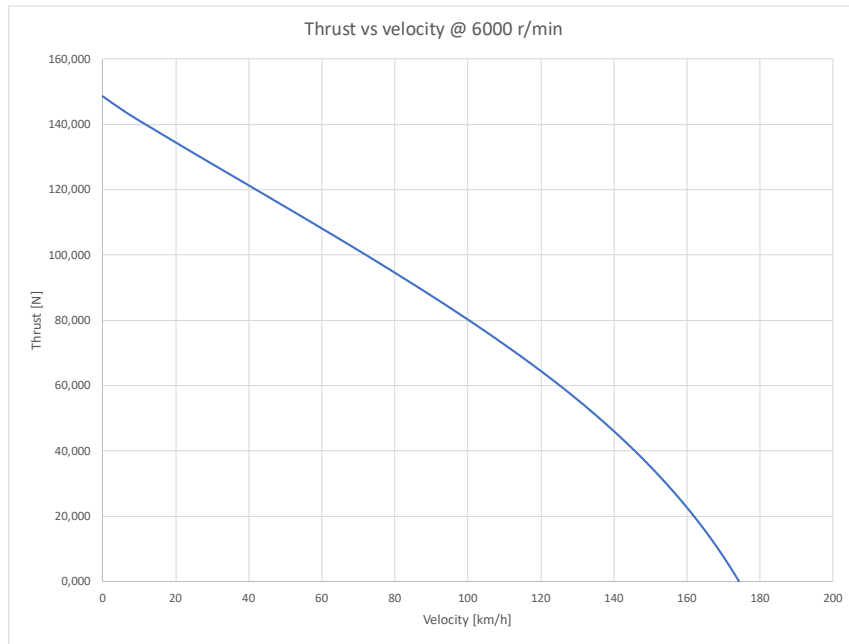


Figure 13 APC 25x12.5E thrust at 6000 r/min as a function of relative air velocity [APC propellers]

In Figure 14 is plotted thrust required for take-off run and rotational speed needed to achieve this. The thrust is set so that take off is possible in approximately 15s. The RPM figures are derived from the manufacturer’s wind tunnel tests data for the chosen propeller.

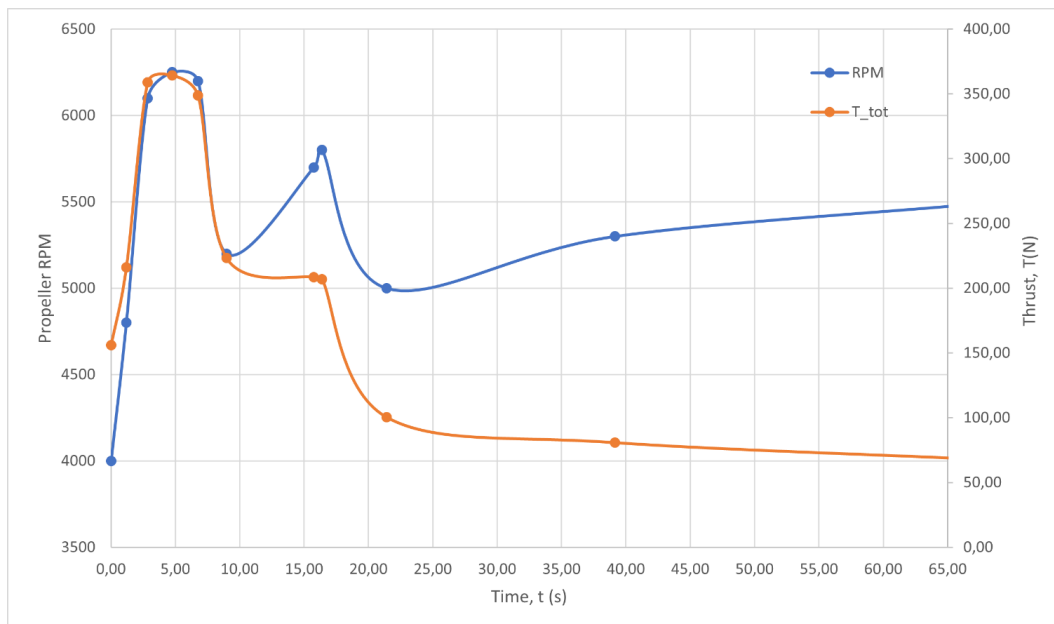


Figure 14 RPM and thrust required of A-1 at different stages of flight. [APC propellers, Deliverable D3.1]

For cruise flight at speed of 108 km/h constant 5000 RPM is appropriate. At landing thrust is needed just enough to keep the craft airborne until touch down, for which some 3500 RPM is sufficient.



## 4.2 Electric motor requirements

Choosing the right electric motor for Airship involves various factors such as power requirements, efficiency, weight, and size constraints.

Based on the preliminary simulations, the selected motor must be capable to provide both the required combined continuous power (1.5 – 3.5 kW) and the peak power rating (2.7 – 4.5 kW), considering that the aircraft will be outfitted with two motors. An additional desirable characteristic of the motor is the ability to deliver power in a manner compatible with the propeller, ensuring that it can provide torque at the propeller's designated rotational speed, avoiding the need for a gearbox and thus reducing overall complexity and weight.

As an electric aircraft, it is important to maximize the motor's efficiency, even though particular efficiency specifications are not provided. This optimization would translate to either a diminished battery size, an extended range, or increased payload capacity for a given battery.

In aircraft design, where weight reduction is crucial, selecting the lightest possible motor is essential. This consideration makes the choice of motor technology crucial.

Considering aerodynamic efficiency, the selected motor should not only prioritize weight reduction but also volume, being as compact as possible.

Commercial availability plays a significant role in motor selection. Certain types of motors are better suited for specific applications, leading to a natural inclination of the market towards particular technologies. This alignment between motor characteristics and application requirements influences the prevalent choices in the commercial field.



*Figure 15 Candidate BLDC motor for AIRSHIP-1 prototype*

Taking all factors into account, the brushless DC motor, especially in the outrunner configuration, stands out as the optimal choice. It demonstrates the capability to meet the specified power requirements, enabling direct drive while minimizing the impact on both weight and aerodynamics in the realm of electric aircraft propulsion. Widely proven in air modelling, the main drawback lies in the fact that commercially available BLDC motors typically operate at voltages significantly lower than the microgrid's rated 400 volts.



A candidate motor for this application could be the Hacker A60-20 M V4 kv170, as it can deliver the preliminary required performance (2744W when equipped with an 21x13 propeller) with a moderate weight and dimensions small enough to fit in the space inside the bodywork provided in the 3D model. An overview of the motor specifications is given in the following table. It is important to point out that the final motor for AIRSHIP-1 cannot be selected yet since accurate aerodynamic and hydrodynamic models and tests must be done before defining the final motor specs.

Table 4 Motor specifications

Motor	Power (W)	Operating voltage (V)	Operating current (A)	Diameter (mm)	Length (mm)	Weight (g)
A60-20 M V4 kv170	2744 at 6010 rpm	38	72	59	75,2	760

Each of these motors require electronics, both for their control and for transforming the DC current into the waveforms shown in Figure 12. Although it could be designed, the most straightforward option would be to purchase one of the commercially available controllers. Being so, the proposed controller is the JETI SPIN 75 Pro OPTO, capable of handling the power demands of the motor.

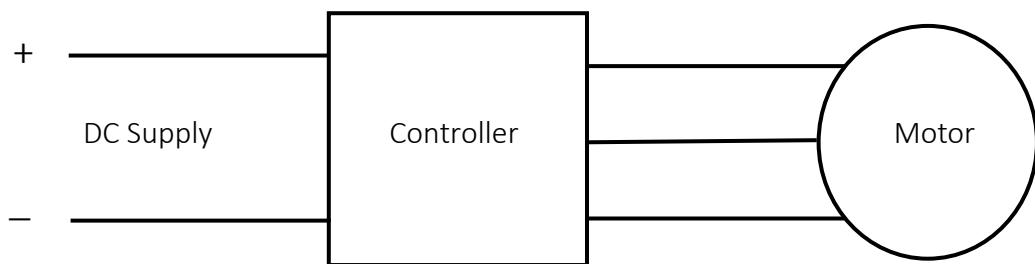


Figure 16 Block diagram: Motor and its controller

An overview of the controller specifications is given in the following table.

Table 5 Controller specifications

Controller	Operating voltage (V)	Input current max (A)	Dimensions LxBxH (mm)	Weight (g)
SPIN 75 Pro OPTO	12 - 42	75	52x25x12	56

As discussed above, for simplicity, a constant pitch propeller will be implemented in the A-1 prototype, and consequently the control of the rotational speed will be done by means of the control of the induced voltage.



### 4.3 DC Microgrid Architecture

The most critical factor to compare different microgrid configurations is the weight, which is detrimental to system redundancy; the more components and redundancy the grid integrates, the heavier the system will be. As mentioned above, the main goal of the DC Microgrid is simplicity and robustness to make sure that the needed energy and power is available and properly delivered during the different operation modes. This microgrid integrates the above-mentioned DC brushless motors as well as the main propulsion. The voltage of the propulsion bus has been adjusted and scaled down to meet the requirements of the prototype and not over-complicate the design. There is an independent secondary 24V bus for control and avionics. In the unlikely event that the propulsion system fails, the avionics and flight control systems would be still properly supplied thanks to the isolated control bus, being possible to enter in emergency mode and to execute landing orders to bring the prototype to safety.

The proposed architecture for the Airship-1 prototype is shown in the following figure. Like the D1 option presented above, it consists of a radial 72 or 48V radial microgrid integrating both DC motors and their controllers with the propulsion battery and the independent secondary battery for the control system. The energy specifications of both grids are similar. Flight control and avionics are expected to demand 1.2kW, so their battery must be dimensioned according to this and keeping the weight constraints of the model in mind. The propulsion battery also needs to be chosen considering the power and energy requirements of the motors during peak demand (taking off and landing) and the steady state flight time which average power demand is expected to be an average of 4kW, peaking at 4.5kW during take-off. Selection of the batteries will be discussed in the Energy generation and storage requirements below.

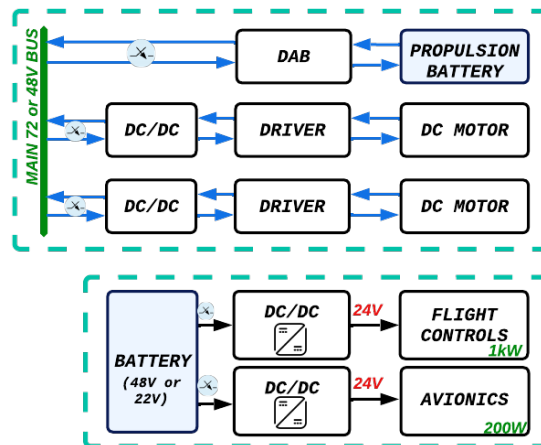


Figure 17 AIRSHIP –1: Proposed DC Microgrid Architecture

Protections and fault isolation is another critical factor when it comes to designing a DC microgrid, this model aims for simplicity and robust design, and control and fault management play a crucial role in achieving that goal. Therefore, control techniques and DC protection measures will also be discussed below.

### 4.4 DC Microgrid dynamic requirements.

In this section it is analysed the dynamic requirements and the stability of the DC microgrid and their effects on the control techniques to meet these requirements.



To control the power and ensure the stability of the grid, two types of control are proposed, one is the current control, and another is the voltage control. In Figure 18, the proposed DC/DC converter is shown, typically called Dual Active Bridge (DAB), where  $V_1$  is the voltage of the battery side and  $V_2$  is the voltage of the DC grid side. The current controller loop must be fast in order to follow the dynamics of the current, on the other hand, and to maintain the DC bus voltage ( $V_2$ ), a slower controller is required.

Respecting current controller two solutions are proposed, the first one based on classical PI linear control, and consequently a high bandwidth is required to follow the fast dynamics, and the second one based on Lyapunov nonlinear control techniques.

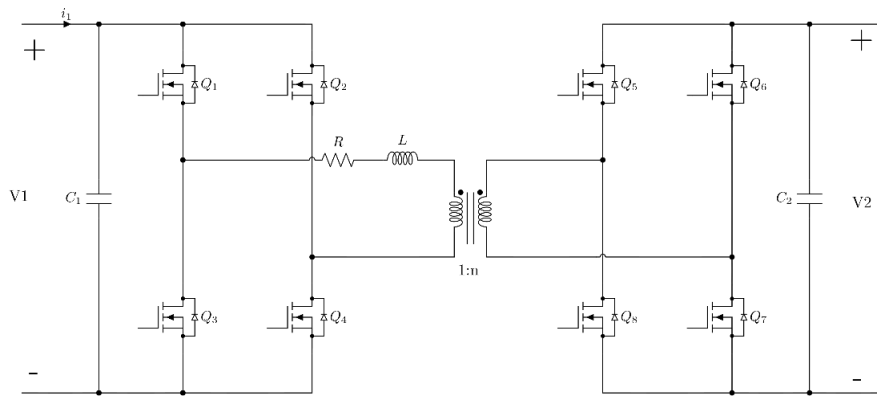


Figure 18 Dual active bridge (DAB) DC/DC bidirectional converter

#### 4.4.1 Current control

Two different control techniques are analysed, the first is based on linear control and the second one is a non-linear control able to improve the dynamic response of the system.

##### 4.4.1.1 PI control

The PI controller is firstly proposed as it does not have error in steady state operation. To control the input current of the DAB, the first step is to linearize the nonlinear circuit model at operating point. The dynamic of the input current ( $i_1$ ) is given by the equation (Jiménez Carrizosa, 2015):

$$\frac{di_1(t)}{dt} = -\frac{R}{L}i_1(t) + \frac{RV_2}{nfL^2}\phi(1 - 2|\phi|) \quad (2)$$

where the  $\phi$  is the phase shift ratio, and  $n$  the transformer turns ratio.

The average circuit is shown, where  $\langle I_1 \rangle$  is the linearized current of input current which ( $i_1$ ).

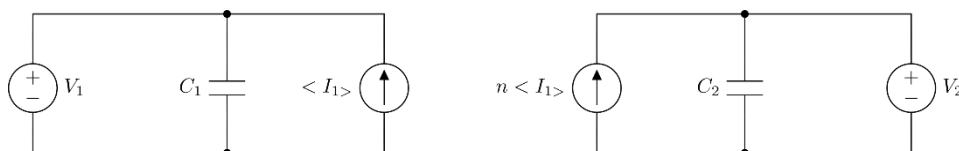


Figure 19 Average circuit of Dual active bridge (DAB) DC/DC bidirectional converter



Table 6 DAB converter specifications for A1

	Value
Battery voltage	72 V
DC grid voltage	400 V
DAB nominal power	1.5 kW
Switching frequency	300 kHz
Maximin current (battery side)	20.84 A

Hence, the transfer function that relates the input current to phase shift ratio is, taking in account the values of Table 6 is:

$$\frac{I_1(s)}{\phi(s)} = \frac{83.38}{0.00014443s + 1} \quad (3)$$

Therefore, the PI controller is designed to have a 1250Hz bandwidth and 85.8° of phase margin, as Figure 20 shows:

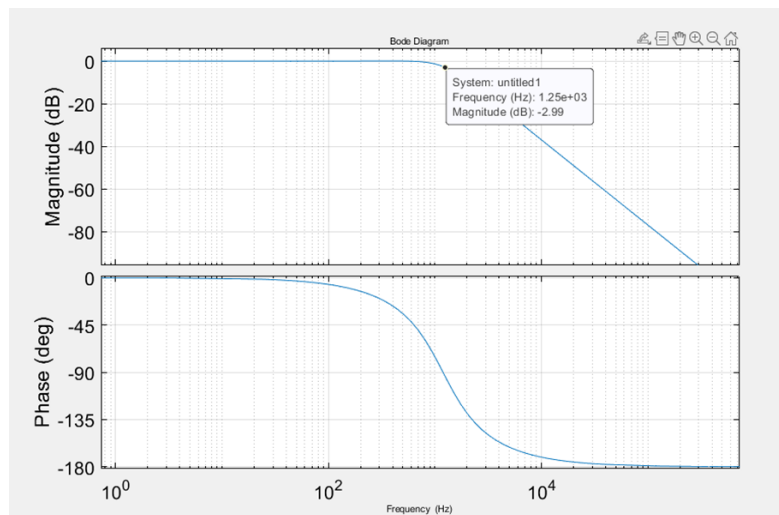


Figure 20 Bode analysis for the current PI controller

Figure 21 shows how is the input current behaves when the current reference is changing from 30A to 30A with a 10A step. The green wave is instantaneous value of the input current, and the red line is the average value of the input current.



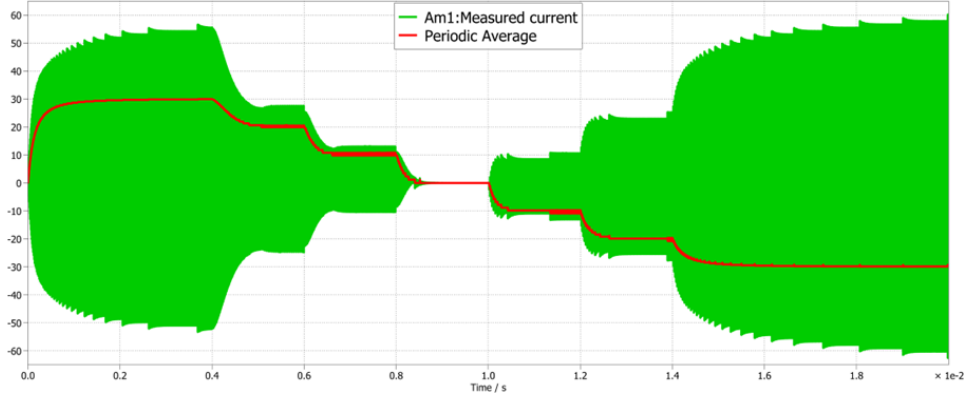


Figure 21 DAB input current simulation with PI controller

However, the traditional PI controller is based on a fixed gain which is around the operating point, so that it cannot ensure the stability of the control over the entire power transmission range. For fast dynamic requirements, it would not be feasible to adjust the gain in real time. Therefore, the nonlinear control is proposed.

#### 4.4.1.2 Nonlinear control

The nonlinear control is based on Lyapunov theory (Khalil, 2002). To track the current reference, we defined the Lyapunov energy function as:

$$V_{(i_1)} = \frac{1}{2} (\langle i_1 \rangle - \langle i_{1,ref} \rangle)^2 \quad (4)$$

To satisfy the stability condition, its time derivative needs to be negative. It is chosen:

$$-\frac{R}{L} \langle i_1 \rangle(t) + \frac{RV_2}{nfL^2} \phi(1 - 2|\phi|) - \frac{d}{dt} \langle i_{1,ref} \rangle(t) = -\alpha \overline{\langle i_1 \rangle}^2 - \beta \overline{\langle i_1 \rangle} \int \overline{\langle i_1 \rangle} \quad (5)$$

where  $\overline{\langle i_1 \rangle} = (\langle i_1 \rangle - \langle i_{1,ref} \rangle)$  is the error, and  $\alpha$  and  $\beta$  two positive tuning gain parameters. If  $K$  is defined as follows:

$$K = \frac{nfL^2}{RV_2} \left[ -\alpha \overline{\langle i_1 \rangle}^2 - \beta \overline{\langle i_1 \rangle} \int \overline{\langle i_1 \rangle} + \frac{R}{L} \langle i_1 \rangle(t) + \frac{d}{dt} \langle i_{1,ref} \rangle(t) \right] \quad (6)$$

and due to the absolute value, there are two cases for solution of phase shift ratio  $\phi$ , depending on the sign of the current reference. The solution is given by:

$$\begin{aligned} \phi &= \frac{1 - \sqrt{1 - 8K}}{4} \text{ if } \langle i_{1,ref} \rangle(t) > 0 \\ \phi &= \frac{-1 + \sqrt{1 + 8K}}{4} \text{ if } \langle i_{1,ref} \rangle(t) < 0 \end{aligned} \quad (7)$$

Finally the control drives the current to track its reference by modulating the phase shift ratio:

$$\phi = \frac{1 - \sqrt{1 - 8K}}{4} S_1 + \frac{-1 + \sqrt{1 + 8K}}{4} S_2 \quad (8)$$



where  $S_1$  is 1 if the  $K > 0$ , and 0 otherwise. And  $S_2$  is 1 if the  $K < 0$ , and 0 otherwise.

The following figure shows the simulation result of the nonlinear control, changing the current reference from 25A to -25A with a 5A step. The green wave is instantaneous value of the input current, and the red line is the average value of the input current.

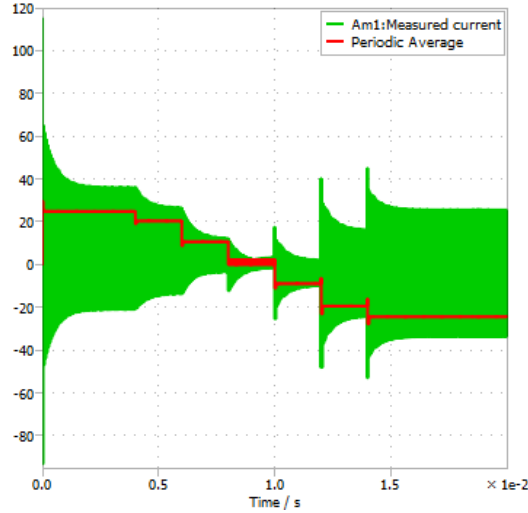


Figure 22 DAB input current simulation with nonlinear controller

#### 4.4.2 Voltage control

The voltage controller is designed to obtain a constant output voltage as the DAB is connected to the DC bus. By comparing the measured voltage with its reference, the controller will provide the current reference for the inner current control loop to provide the power that is demanded by the load. Since the DAB with resistive load can be considered approximately as a first-order system, the PI controller is proposed for the voltage control.

Hence the transfer function that relates the output voltage to the input current is:

$$\frac{V_2(s)}{I_1(s)} = \frac{R_{load}}{n \cdot R_{load} \cdot C_2 \cdot s + n} \quad (9)$$

The voltage controller is designed to have a 145Hz bandwidth and 126.6° phase margin as shown in the Figure 23, with  $K_{pv}=0.1$  and  $K_{iv}=39.26$ .



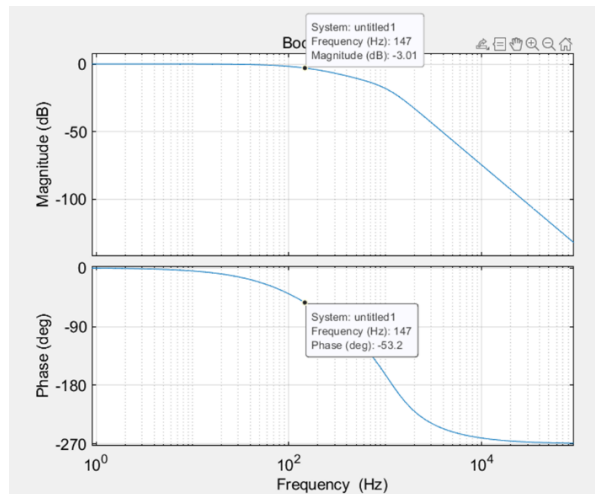


Figure 23 Bode diagram for voltage controller

The simulation results are shown in Figure 24 and Figure 25. In Figure 24, the voltage of DC grid is shown with reference changes from 400V to 300V, and later it goes back to 400V, where the green line is the instantaneous value of output voltage and the red one the reference.

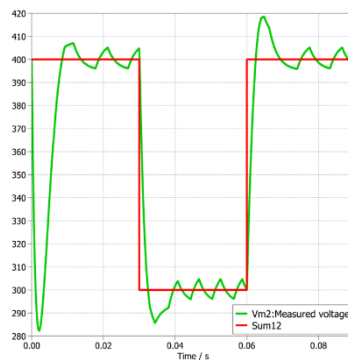


Figure 24 Voltage of DC grid in voltage control mode

In Figure 25, the input current ( $i_1$ ) of DAB is shown, where the green wave is instantaneous value of the input current, and the red line is the average value of the input current



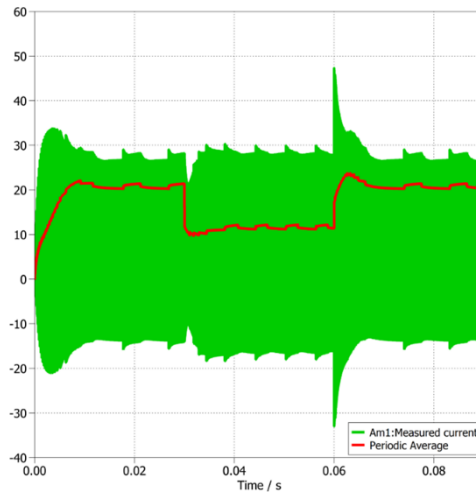


Figure 25 Input current ( $i_1$ ) of DAB in voltage control mode

To validate the proposed control in order to provide power to the load correctly, a simulation with 4 DAB is made (see Figure 26). Two of the DAB is under current control which will demand power from the grid, and another two DAB is under the voltage control which will send the power to the load.

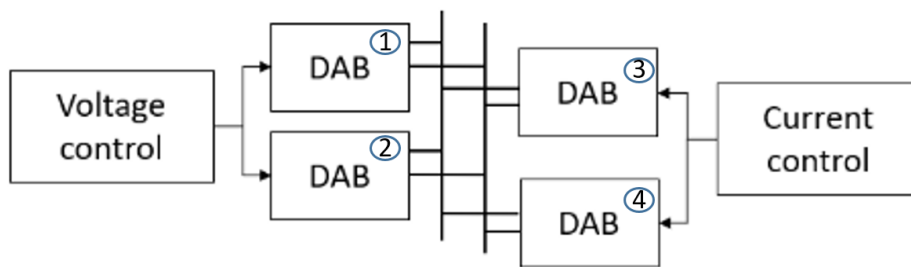


Figure 26 Four nodes DC grid

The results are shown in Figure 27. Firstly, the loads (nodes 3 and 4) are consuming each one 720W, and then, the power consumption steps to 1500W in both nodes. Due to the symmetrical configuration of the proposed four nodes grid, only the input current of nodes 1 (generator) and 3 (load) are shown (the positive current shows the DAB under the voltage control is sending the power and the negative value shows the DAB under current control is consuming power as loads).



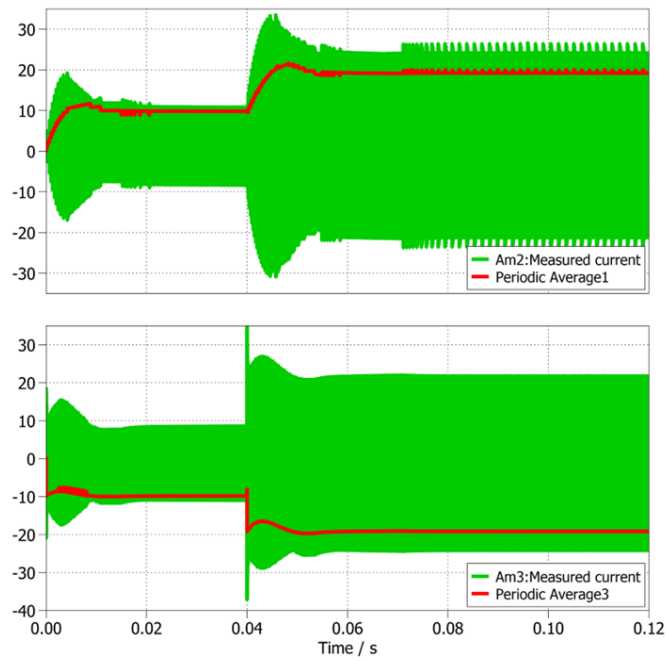


Figure 27 a) Input current of DAB 1 b) Input current of DAB 3

The behaviours of the output voltage are:

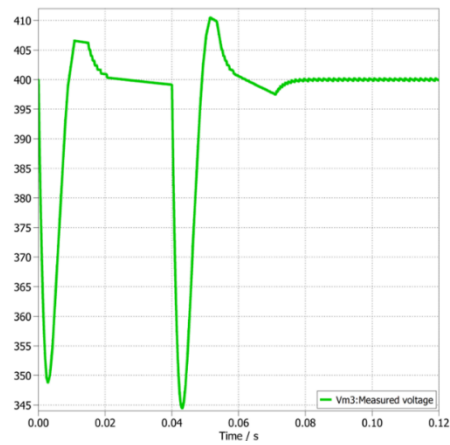


Figure 28 Voltage of the DC grid in the four nodes grid simulation



## 4.5 Energy generation and storage requirements

The requirements for the energy system are based on the power consumption during a flight:

Table 7 Power consumption

<b>Navigation power demand</b>	1.2 kW
<b>Take off /landing time</b>	20s
<b>Take off power</b>	Up to 4.5 kW
<b>Flight time</b>	10 min
<b>Cruise power</b>	Up to 3.5 kW

As shown in Figure 17, two independent grids will form the electrical system, one to supply the flight control and the avionics and the second grid will feed the propulsion system. Each one will have a battery as the only energy source. As this prototype is more focused on testing the mechanical design and to get information from the different sensors and see how the different actuators affect the behaviour of the UAV, the electrical system is specified as simple as possible. It is also important to note that, the peak power to average power consumption ratio is low (about 1.3), therefore it is not necessary to include super capacitor to smooth the battery current demand, as this ratio is affordable for a battery. In this case study, voltage and current sensors will be included to record the power consumption of the different elements and adjust the energy generation and storage system to more precise specifications.

- Navigation system battery: The main specifications for this element are listed below assuming a 95% efficiency in the system.

Power	1.3 kW
Energy	225 Wh

Different technologies and configurations have been studied as show below.

Table 8 Analysed commercial batteries for the Navigation and control system

Battery		Vnom	Vmin	Energy (Wh)	Capacity (Ah)	Total volume (cm3)	Total weigth (kg)	Payload %	Maximum current (A)
Bat1	IonLi	72	60	2100	30		15,5	70,4	20
Bat2	LiPo	22,2	18	115,44	5,2	8122,4	1,6	7,3	260
Bat3	LiPo	3,7	3	0,296	0,08	1198,08	1,58208	7,2	76,8
Bat4	IonLi	72	60	3024	42	7400	14	63,6	100
Bat5	IonLi	60	48	720	12	1790,25	3,2	14,5	30
Bat6	IonLi	48	39	2160	45	6247,5	9,5	43,2	70
Bat7	IonLi	48	39	1200	25	5088,75	8,6	39,1	100
Bat8	LiPo	51,8	42	880,6	17	4593,15	4,4	20	357
Bat9	LiPo	58,8	42	940,8	16	2031,12	4,3	19,5	178,5
Bat10	LiPo	58,8	42	282,3	5,45	776,79	1,597	7,3	163,5



The best alternative is the last one listed, an LiPo battery of 5450mAh capacity, its weight is around 7% of the payload.

- Propulsion system battery: The main specifications for this element are listed below assuming a 95% efficiency in the system.

Peak Power	4.5 kW
Energy	810 Wh

As in the previous case different alternatives have been analysed.

*Table 9 Analysed commercial batteries for the Propulsion of AIRSHIP-1 demonstrator*

Battery		Vmon	Vmin	Energy (Wh)	Capacity (Ah)	Total volume (dm <sup>3</sup> )	Total weight (kg)	Payload %	Maximum current (A)
Bat1	IonLi	72	60	2100	30		46,5	232,5	60
Bat2	LiPo	22,2	18	115,44	5,2	24367,2	4,8	24	390
Bat3	LiPo	3,7	3	0,296	0,08	3519,36	4,6	23,2	225,6
Bat4	IonLi	72	60	3024	42	7400	14	70	100
bat5	IonLi	60	48	720	12	7161	12,8	64	60
bat6	IonLi	48	39	2160	45	12495	19	95	70
bat7	IonLi	48	39	1200	25	10177,5	17,2	86	50
bat8	LiPo	51,8	42	880,6	17	4593,15	4,4	22	357
bat9	LiPo	58,8	42	940,8	16	4062,24	8,6	43	178,5

In this case, the best alternative for the propulsion grid is the bat8 battery, an LiPo battery of 17000mAh capacity, its weight is around 22% of the payload.

As conclusion the energy system for the A1 prototype is based on LiPo batteries, and its weight is around 30% of the admissible payload of the UAV.

## 4.6 DC protections

Current protections consist of two main areas:

- Fault detection and classification
- System response: isolation of the section under fault.

Safety control may be carried out by a dedicated circuit, while the system response must be carried out by the system elements, namely circuit Breakers or the DC/DC converter itself.

There are several DCCB (DC Circuit Breakers) typologies, including fully mechanical switches, hybrid setups, and fully Solid-state circuit breakers.

The following figure shows an example of a Solid State DC Circuit Breaker (SSCB). It must be noted that the capacitor of the resonant circuit must be charged for correct operation, either by the circuit itself or an additional external charger.



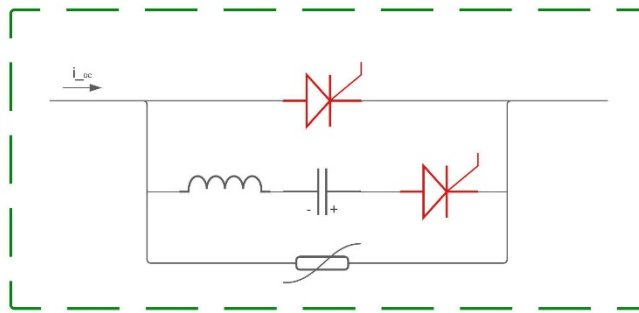


Figure 29 Solid State DC Circuit Breaker

SSCB, compared to mechanical circuit breakers (MCB) or hybrid circuit breakers (HCB) allow for self-charging, compactness, and good response times at the cost of slightly worse efficiency (caused by the solid-state switch's ON-state resistance).

#### 4.6.1 Fault detection

The main parameters to be considered are system currents and their derivatives. In DC systems, faults can be classified into pole to pole (PP) and pole to ground (PG) faults. Consequently, protections must be able to distinguish between them at all foreseeable load levels and implement the appropriate response. Moreover, it must be robust against false positives in normal operation and sudden changes in load conditions.

There are multiple possible approaches to fault detection and classification, including impedance-based detection, travelling wave protection schemes, or Artificial neural network usage. It is important to note that we are restricted in the protection system's weight, power requirements, and redundancies.

#### 4.6.2 System response

Once a fault has been detected, the system must respond appropriately to reduce the current in the affected area and isolate the circuit. This is best achieved using SSDCCB (solid-state DC breakers) positioned as seen in section 4.3, which reduce the current and dissipate energy until the node can be physically disconnected from the grid.

Some fault scenarios would be:

- Detection of unusually high current (or oscillations) in one of the secondary branches.
- Sudden voltage drop indicating a fault to ground in one of the branches.
- Fault in power supply. In this case on top of setting off the breakers the DAB's own internal protections must force it to stop forwarding current to protect internal components.



## 5 Full DC Microgrid Architecture for AIRSHIP A-1: Lab demonstrator

As mentioned above, from the Power Plant perspective the DC microgrid developed to be installed on-board of AIRSHIP-1 prototype will be the basic one to guarantee the proper energy and power delivery under the different flight tests. This basic DC Microgrid includes only batteries as storage technology but does not integrate other technologies like Fuel Cells or Supercapacitors that would allow to optimize the size and weight of the whole DC Microgrid.

A whole DC Microgrid architecture for AIRSHIP project will be developed and validated through an off-board Lab demonstrator that will integrate all the needed technologies for a zero net emissions and self-sustainable DC Microgrid. This Lab demonstrator integrates Fuel Cell and Supercapacitors technologies to minimize the size and weight of the on-board energy storage elements as well as off-board PV panels and electrolyser to reach a zero net emissions demonstrator.

### 5.1 DC Microgrid Architecture

Taking into account robustness and redundancy, radial architecture including redundant batteries and fuel cells (Architecture C2) is a very appropriate candidate for this demonstrator. The radial configuration provides a simple approach for controlling and monitoring the main bus; implementing DC breakers in series with the converters on each node provides a higher security layer. The energy stored among batteries and fuel cells is not double, it is just the energy required for the flight test; then redundant batteries and fuel cells does not double the energy requirements but make the system tolerant to one failure, being able to keep working even under the fault of one of the battery or fuel cell branches.

The connection to the off-board electrolyser is made via pressure valves, and the option to connect to the electrical port grid is open to consideration and presents an opportunity to re-fuel the hydrogen tanks from renewable energies like solar energy from the PV panels.

As the aim for this Lab demonstrator of the Full DC Microgrid is to validate the integration of the technologies that can be implemented in a real Air Ship, the microgrid is designed expecting a higher power demand. Integrating all the initially proposed renewable energy generation and storage systems. Therefore, 400V is the selected voltage for the DC bus since it allows to handle and integrate higher power levels.

Besides, 400V DC Bus allows to integrate PMSM motors that would be the appropriate motors for a real Air Ship. Motor nodes depend on the implemented drivers, DC/DCs would be optional if the drivers could not handle the 400V bus voltage.



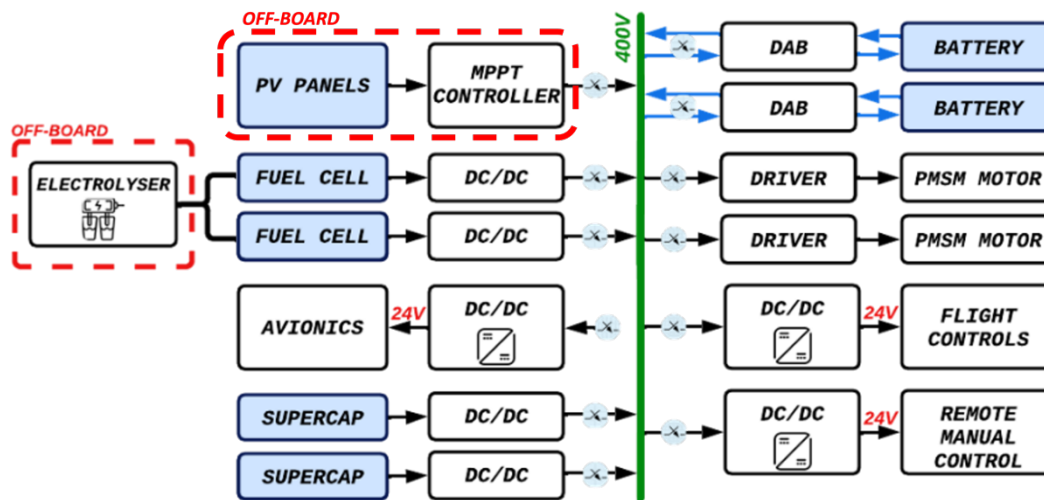


Figure 30 Full DC Microgrid Architecture for AIRSHIP-1: Lab demonstrator

Microgrid specifications are calculated for the 400V bus under peak energy demand during take-off and landing, ensuring robust performance during steady state flight conditions.

As the motors implemented for this model are PMSM, the motor node will need a DC/AC unit, which can be implemented or not in the motor controller, this will depend on the chosen model.

## 5.2 Energy generation and storage requirements

In this section the scaled version of the energy generation and storage system will be described. The main objective is to build a microgrid that would include all the elements proposed for the commercial concept and test the control algorithms in the Lab micro grid. This Lab system will be based on the A1 power and energy consumption. The specifications are listed in the table below.

Table 10 Power consumption in A-1

Navigation power demand	1.2 kW
Take off /landing time	20s
Take off power	Up to 4.5 kW
Flight time	10 min
Cruise power	Up to 3.5 kW

The elements of this Lab microgrid are the ones shown in Figure 30. The energy storage will be share between two batteries and two fuel cells, as a preliminary proposal, each battery and cell will store a 25% of the required energy. Supercapacitor will be included to have an extra 5% energy in case of peak power demand.



The PV panels will be sized to generate the energy needed in 2h of operation.

- **Batteries:** Two batteries will be included in the Lab microgrid. The energy requirements for the batteries are:

Energy (Wh)	Pmax (kW)
222,807018	1,425

As in section 4.5, several alternatives have been analysed:

Table 11 Analysed commercial Batteries for the Lab Demonstrator

Battery		Vnom	Vmin	Energy (Wh)	Capacity (Ah)	Total volume	Total weight	Payload %	Maximum current (A)
Bat1	IonLi	72	60	2100	30	0	15,5	70,5	20
Bat2	LiPo	22,2	18	115,44	5,2	8122,4	1,6	7,3	130
Bat3	LiPo	3,7	3	0,296	0,08	1198,08	1,58208	7,2	76,8
Bat4	IonLi	72	60	3024	42	7400	14	63,6	100
Bat5	IonLi	60	48	720	12	1790,25	3,2	14,5	30
Bat6	IonLi	48	39	2160	45	6247,5	9,5	43,2	70
BAt7	IonLi	48	39	1200	25	5088,75	8,6	39,1	100
Bat8	LiPo	51,8	42	880,6	17	4593,15	4,4	20	357
Bat9	LiPo	58,8	42	940,8	16	2031,12	4,3	19,5	178,5
Bat10	LiPo	58,8	42	282,3	5,45	776,79	1,597	7,3	163,5
Bat11	LiPo	66,6	54	23,22	0,43	1073,1	2,19	10,0	75,25
Bat12	LiPo	66,6	54	36,18	0,67	1365,552	2,64	12	69,68
Bat13	LiPo	66,6	54	249,75	3,75	708,975	1,662	7,6	142,5

- **Fuel cells:** As the energy storage will be equally shared between the energy storage elements the requirements for the fuel cell are the previous listed for the batteries. Analysing the alternatives present in the market is expected to select a fuel cell with the following characteristics:

Table 12 Fuel Cell specifications for the Lab Demonstrator

Vcell (mV)	Pcell (W)	Coolant	Flow rate (slpm/cell <sup>2</sup> )	Ncells	Total volume (cm <sup>3</sup> )	Total weight (kg)	Payload %
660	41.1	Air	30	37	8670	7.26	36

It is important to note that the energy density of this specification is far away from the energy density of the fuel cells of commercial vehicles where there are power densities around 0.67 kW/kg, but as this grid is not planned to be mounted in any vehicle and its main purpose is to validate the integration of the different technologies and to test the control algorithms to regulate the grid, therefore the power density of each element is not crucial.

- **Supercapacitor:** As shown in Figure 30, the microgrid has two independent supercapacitors therefore each one should have an energy capability of 2.5%



Energy (Wh)	Pmax (W)
22,3	150

Based on the solutions present in the market, the main characteristics for the supercapacitor are listed in the following table.

Table 13 Supercapacitors specifications for the Lab Demonstrator

Vmax (V)	C (F)	Stored energy (Wh)	Total weight (kg)	Payload %
170	7.9	26.6	6	30

As in the case of the fuel cells, this element is not optimized for the UAV, and its final specification will be given once the average consumption and peak power demanded by each of the elements connected to the microgrid are known with greater precision.

- PV panels:** The scaled PV plant should generate enough power to recharge the batteries and, as this UAV is planned to be zero net emission, the H<sub>2</sub> must be generated using a renewable energy source. Therefore, PV panels also have to supply the electrolyser. Assuming that the average power generation per square meter of a PV panel is around 180W. The efficiency of the power converter to interconnect the different element is estimated about 95%. And limiting up to 2h the available time to generate the energy needed to recharge the batteries and to generate the H<sub>2</sub> to refill the tanks. Estimating the efficiency of the production of green H<sub>2</sub> and the efficiency of the fuel cell based on commercial solutions. The total area needed is 6.3 m<sup>2</sup>.

Table 14 PV panel design

Element	Value
Batteries energy	445.6 Wh
Fuel cell energy	445.6 Wh
Fuel cell efficiency	50%
Electrolyser efficiency	54%
Total energy needed	2.2 kWh
Time	2 h
Solar power production	1.1 kW
PV panel area	6.3 m <sup>2</sup>

### 5.3 Full DC Microgrid: Dynamic requirements and grid stability

To analyse the dynamic requirements of the full DC Microgrid where all the technologies are integrated, the DAB converters has been modelled and control as proposed in section 4.4. The following figure shows the simulated DC Microgrid.



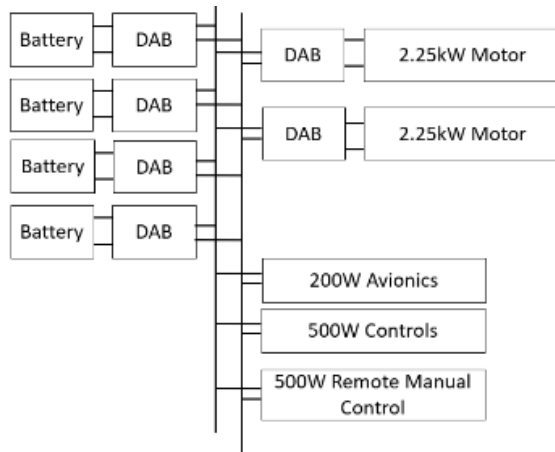


Figure 31 DC Microgrid architecture modelled to analyse dynamic requirements

### 5.3.1 Taking off

The grid simulation during the taking off is made as the motor power consumption is changing in a big range. The total power of the control system is constantly 1.2kW which consists of 200W in avionics, 500W in controls and 500W in remote manual control. For the propulsion, the power will increase linearly to 4.5kW in total for 2 motors. In the simulation the taking off time is scaled to 0.4s to reduce the memory requirement of simulation.

Figure 32 shows the DAB current behaviour. The green wave is instantaneous value of the input current, and the red line is the average value of the input current. The positive current shows the current behaviour at the battery side and the negative current shows the current at motor side.

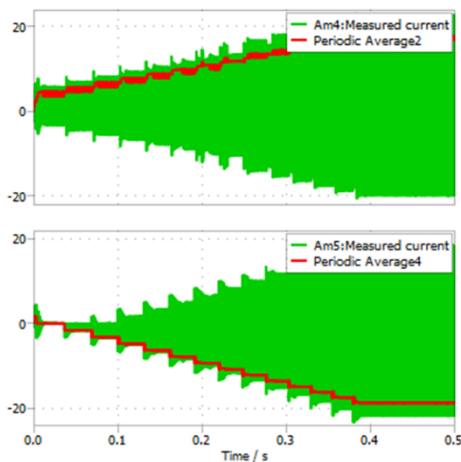


Figure 32 Input current of the DAB converter within the Full DC Microgrid simulation during the take off.

Figure 33 shows the Bus voltage dynamics while the power consumption is increasing.



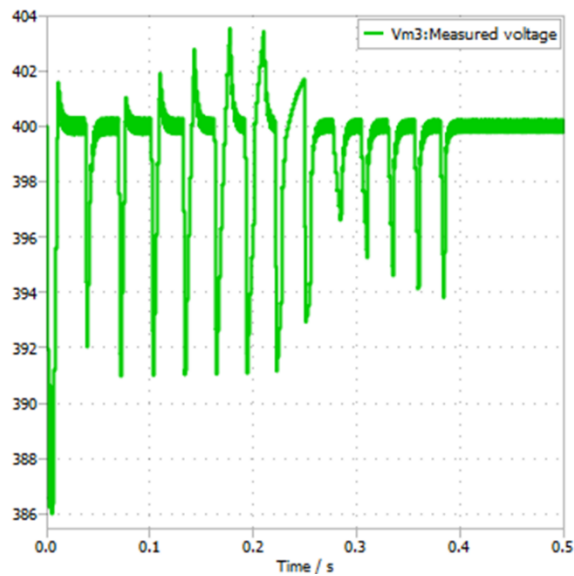


Figure 33 Voltage of the DC Bus within the Full DC Microgrid simulation during the take off.

### 5.3.2 Cruise

The power consumption during the cruise is constant and the converters operate at steady state. The current waveform of the DAB current is shown below. The green wave is instantaneous value of the current, and the red line is the average value of the current. Positive current is the input current of the DAB under voltage control which provides power constantly. The negative current indicates the motor is consuming a constant power.

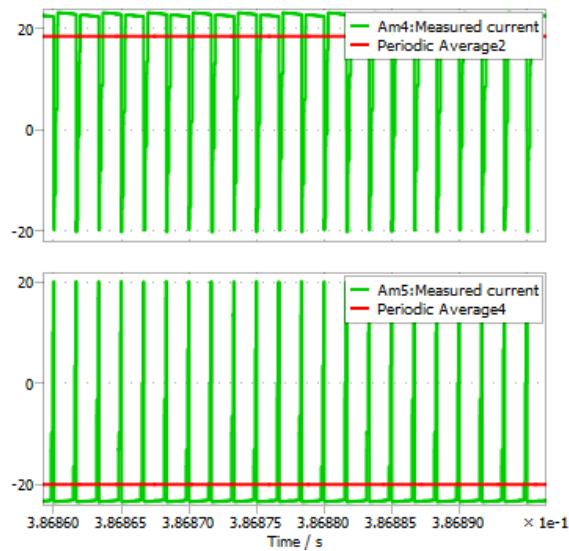


Figure 34 Input current of the DAB within the Full DC Microgrid simulation during the cruise.

The following capture shows the DC bus voltage which is 400V constantly.



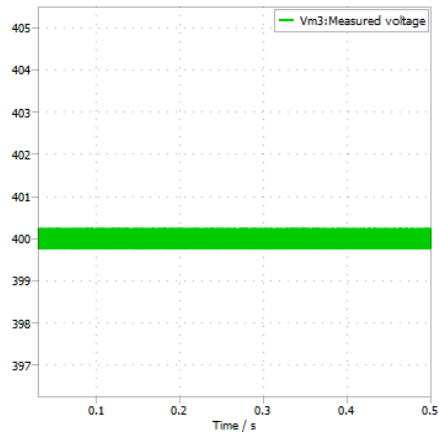


Figure 35 Voltage of the DC grid within the Full DC Microgrid simulation during the cruise.

### 5.3.3 Landing

The simulation of the landing is made as the power demanded by the motors decreases from the maximum power to zero. Therefore, the current in the motor is decreasing during the landing process and the input current of DAB that provides power will reduce tracking this change. The results are shown in the following figure.

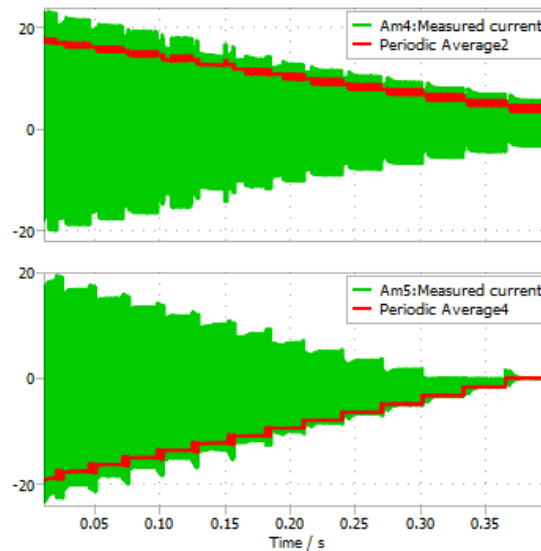


Figure 36 Input current of the DAB within the Full DC Microgrid simulation during the landing.

## 5.4 DC protections and redundancy

A more thorough analysis is yet to be carried out to determine the most likely faults and most appropriate responses in the commercial scale model. The general design philosophy for protections in the commercial concept is similar the one explained in section 4.6 for the AIRSHIP-1 prototype. In a severe accident resulting in loss of power to the motors, priority should be given to flight control systems which may attempt an emergency landing.



## 6 Conclusions

Two demonstrators of the Propulsion DC Microgrid has been defined and specified to be developed for the AIRSHIP-1 scenario:

- AIRSHIP-1 on-board DC Microgrid: the main goal of this demonstrator is to deliver on-board the power and energy under all the flying tests. Simplicity and robustness are the main desig drivers.

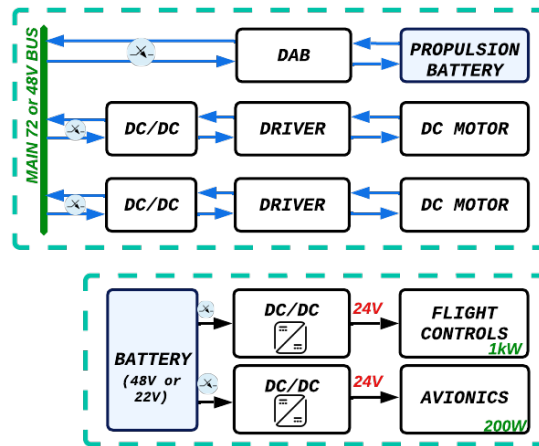


Figure 37 AIRSHIP –1: Proposed DC Microgrid Architecture

- Full DC Microgrid for AIRSHIP-1. Lab Demonstrator: the main goal of this demonstrator is to integrate and validate all the technologies of the propulsion DC Microgrid to be tested in the Lab.

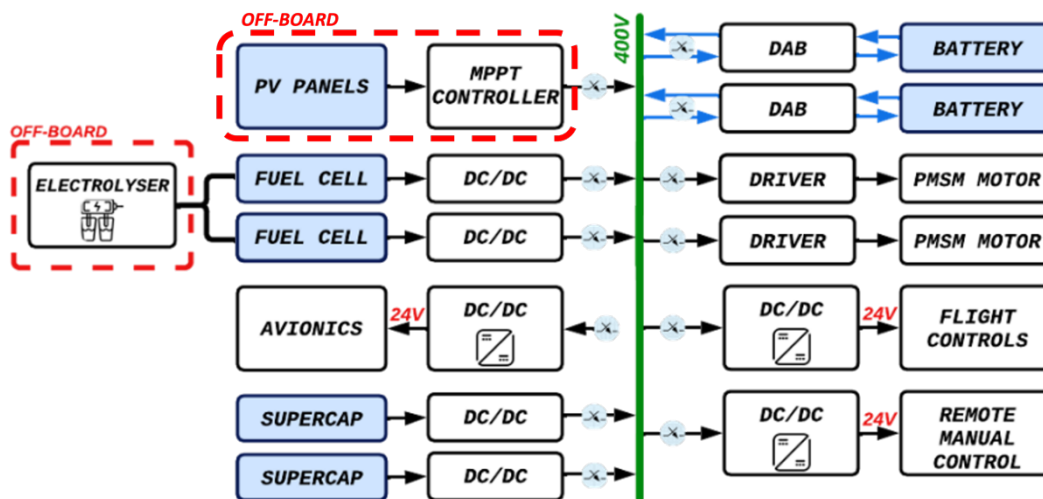


Figure 38 Full DC Microgrid Architecture for AIRSHIP-1: Lab demonstrator



Fuel Cells and Batteries area redundant to increase the reliability of the system. In case of failure detection, the branch under failure can be isolated thanks to the Circuit breaker that is in series with each branch.

The specifications are preliminary since more accurate aerodynamic and hydrodynamic models and tests are to be developed before defining the final specifications.

DC Microgrid architecture is selected for both demonstrators; Radial configuration is selected for both cases accounting for reliability and simplicity.

Dynamic models of the DC Microgrid has been developed to analyse the dynamic behaviour and the stability of the system under take-off, cruise and land operations. Linear and Non Linear controls has been developed to guarantee stability as well as an appropriate response of the system, depending on the final dynamic requirements one of this control approaches will be selected.



## References

[Use the APA citation style – see [https://www.library.cornell.edu/research/citation/apa for details](https://www.library.cornell.edu/research/citation/apa%20for%20details)]

Buchmann, I. (2010). Bu-107: *Comparison table of secondary batteries*. Battery University. [http://batteryuniversity.com/learn/article/secondary\\_batteries](http://batteryuniversity.com/learn/article/secondary_batteries) (accessed 13 February, 2016).

Dragicevic, T. ; Wheeler, P.; Blaabjerg , F (2018) *DC Distribution Systems and Microgrids*, IET Digital Library

Harrison, K. W., Remick, R., Hoskin, A., & Martin, G. D. (2010). Hydrogen production: fundamentals and case study summaries (No. NREL/CP-550-47302). National Renewable Energy Lab.(NREL), Golden, CO (United States).

Heinrich, M., Kuhn, T., Dimroth, F., Würfel, U., Goldschmidt, J. C., Powalla, M., ... & Neuhaus, D. H. (2020). A comparison of different solar cell technologies for integrated photovoltaics.

Jiménez Carrizosa, M., *Hierarchical control scheme for multi-terminal high voltage direct current power networks*, PhD dissertation. Université Paris Sud-Paris XI. April 2015.

Khalil, H., *Nonlinear systems*, Prentice Hall 2002.

Lopez-Alonso, E., Papini, D., Jiménez., G., (2017) Hydrogen distribution and Passive Autocatalytic Recombiner (PAR) mitigation in a PWR-KWU containment type. *Annals of Nuclear Energy* 109, p.600–611.

Mora, J. F. (2016). Máquinas eléctricas. Garceta.

Mevey, J. R. (2009). Sensorless field oriented control of brushless permanent magnet synchronous motors (thesis). Kansas State University, Manhattan, Kan.

The renewable energy hub <https://www.renewableenergyhub.co.uk/main/solar-panels/solar-panel-power-per-square-foot>

US Fuel Cell Council chrome-extension://efaidnbnmnnibpcajpcglclefindmkaj/[https://www.hydrogen.energy.gov/docs/hydrogenprogramlibraries/pdfs/htac\\_fc\\_products.pdf?Status=Master](https://www.hydrogen.energy.gov/docs/hydrogenprogramlibraries/pdfs/htac_fc_products.pdf?Status=Master)

Clean energy reviews <https://www.cleanenergyreviews.info/blog/most-efficient-solar-panels>

Epec engineered technologies <https://www.epectec.com/batteries/cell-comparison.html>

Asian Development Bank <https://www.adb.org/sites/default/files/publication/479891/handbook-battery-energy-storage-system.pdf>

Miao, Y., Hynan, P., Von Jouanne, A., & Yokochi, A. (2019). Current Li-ion battery technologies in electric vehicles and opportunities for advancements. *Energies*, 12(6), 1074.

AIRSHIP-project deliverable D3.1 Conceptual Design Report



Funded by the  
European Union

APC Propellers (<https://www.apcprop.com/>)



Funded by the  
European Union



*Figure 39. EU Flag.*

